Hindawi
International Journal of Aerospace Engineering
Volume 2021, Article ID 8838398, 19 pages
https://doi.org/10.1155/2021/8838398

Research Article

A New Compensation Method for DRR of a Roll-Pitch Seeker Based on ESO

Yue Li,[1] **Wei Li**,[1] **Xiaodong Liu**,[2] **and Qunli Xia**[1]

[1]*Beijing Institute of Technology, Beijing 100081, China*
[2]*Beijing Aerospace Automatic Control Research Institute, Beijing 100854, China*

Correspondence should be addressed to Yue Li; liyue627167955@163.com

Received 29 July 2020; Revised 27 December 2020; Accepted 1 January 2021; Published 15 January 2021

Academic Editor: Giovanni Palmerini

Copyright © 2021 Yue Li et al. This is an open access article distributed under the Creative Commons Attribution License, which permits unrestricted use, distribution, and reproduction in any medium, provided the original work is properly cited.

We propose a new DRR (Disturbance Rejection Rate) compensation method of a roll-pitch seeker based on ESO (extended state observer). The characteristics of a roll-pitch seeker and the DRR definition of two frames of a roll-pitch seeker are analyzed. The influence of different interference torques and different frequency bandwidths on the compensation effect is analyzed. Modeling and simulation of the guidance system of a roll-pitch seeker with the parasitic loop of DRR are carried out. Influence of the new DRR compensation method on dimensionless miss distance is analyzed. Mathematical simulation is established to compare the new ESO-based DRR compensation method with the existing methods such as the feedforward method and Kalman filter method. The analysis and simulation results show that the new ESO-based DRR compensation method has the advantages of high precision, good applicability, and easy adjustment, and the new method can effectively reduce the dimensionless miss distance with different types of input errors. The research of this proposed new method can provide a reference for the latest generation air-to-air missile operations in a high-altitude and high-speed environment and the high-precision research of a roll-pitch seeker.

1. Introduction

Capturing air combat environment control is an important task in modern war, and precision-guided air-to-air missiles play an important role in this task [1–3]. The infrared-guided air-to-air missile has many characteristics such as high precision of guidance, strong target recognition ability, and good concealment. An optical seeker is an important part of an air-to-air missile precision guidance system [4, 5]. An air-to-air missile usually uses a two-frame platform seeker to eliminate missile body disturbance and track the target by means of pitch and yaw frame motion. Due to the structure limitation, the off-axis angle of the seeker cannot be too large, so it is difficult to meet the requirements of the latest generation air-to-air missile [6–8].

The roll-pitch seeker is a new type of structural seeker, which adopts the polar coordinate structure of the rolling outer frame and pitching inner frame [9, 10]. This kind of seeker can achieve a frame angle of ±90°, so that the viewing field of the seeker can cover the whole front hemisphere, which provides the necessary conditions for the missile to launch at a large off-axis angle. It has the large field of view of the platform seeker. At the same time, the roll-pitch seeker adopts a semistrapdown stability control platform, on which no inertial devices are installed. The infrared detector of the roll-pitch seeker is fixed on the missile body, only the optical system is installed on the stable platform, and the incident light is transmitted to the detector through the light path composed of four mirrors [11–13]. This kind of structure not only reduces the size and mass of the seeker but also improves the aerodynamic performance of the missile body. The roll-pitch infrared seeker has the characteristics of infrared imaging guidance, strapdown guidance, large field of view, and miniaturization so that it is very suitable for short-range combat air-to-air missiles [14–16].

The control system of the roll-pitch seeker is mainly composed of two loops: the stability loop and the track loop. The stability loop forms a closed-loop control through the angular velocity feedback of the platform relative to the inertial space to isolate the missile body disturbance. The

interference torques of the seeker include spring torques, friction torques, damping torques, etc. The mass imbalance and the coupling between the frames will also cause interference torques [17, 18]. The existence of interference torque will make the missile body disturbance to be coupled to the line-of-sight angular velocity information. Furthermore, the guidance information output by the seeker will be not accurate, which will seriously affect the missile performance [19]. Therefore, suppressing the bad influence of interference torque on the seeker becomes the key to improve the missile performance.

To solve the problem of the roll-pitch seeker's suppression of interference torque and compensation for DRR, many researchers have proposed some quantitative methods [15, 20–26]. Li et al. [20, 21] take the platform seeker as the research object and propose the DRR compensation strategy based on ESO, which cannot be applied to a roll-pitch seeker without improvement. Liu et al. [15, 22] propose a differentiator-based DRR compensation method for a roll-pitch seeker. In the case of small information transfer error within the frame of a roll-pitch seeker, this differentiator-based compensation method has a positive effect, but when the information transfer error is large, the compensation effect is not so good. Du and Xia [23] propose a feedforward DRR compensation method for a roll-pitch seeker. The compensation effect is good when the feedforward method is applied to the real seeker model. However, when there are errors between the applied model and the real model, the effect of the feedforward compensation method is bad. Liu et al. [24] propose a DRR compensation method based on the Kalman filter, which can be applied to various simulation environments and seeker models. However, this method involves the filtering process, which means that the compensation effect will be affected by the filtering accuracy. Gao et al. [25] propose an estimation and compensation method for engineering application, but it lacks theoretical derivation. Lin et al. [26] proposed an estimation method combining Kalman filtering and ESO, but it was not used in the roll-pitch seeker. The above-mentioned methods [15, 20–26] cannot completely solve the DRR compensation problem of the roll-pitch seeker under different simulation environments. The compensation effect will change with the change of the environment, and the influence of model loop parameters on the compensation effect is not considered in these existing methods either.

We take the roll-pitch seeker as the research object, aim at roll-pitch seeker DRR compensation problem, and propose an improved ESO-based DRR compensation method. The main content of each section is as follows. In Section 1, the DRR compensation problem of the roll-pitch seeker is presented, and several existing DRR compensation methods are listed. In Section 2, the DRR models of different roll-pitch seeker frames are established, and the influence of different types of interference torques on DRR size is analyzed. In Section 3, the ESO-based DRR compensation method is proposed, and the effects of different types of interference torques and different frequency bandwidths on the compensation effect are simulated and are compared with those of the existing methods. In Section 4, the model of the DRR parasitic loop of the roll-pitch seeker is established, and the influence of DRR compensation on the dimensionless miss is simulated in the guidance system with different types of error inputs. In Section 5, the research results and relevant conclusions are given.

2. DRR Model of the Roll-Pitch Seeker

A pitch-yaw seeker is a platform seeker that can directly obtain angular velocity information of the line of sight. Therefore, when defining DRR of the pitch-yaw seeker, the following formula can be directly followed. The concept of DRR is a ratio, and the standard way to describe or contrast DRR is to use percentage. However, in the calculation, it does not matter whether it is written as a percentage or not. To make the theoretical derivation part of our paper more precise, we add a percent sign to the theoretically derived equation.

$$R = \frac{\dot{q}(s)}{\dot{\vartheta}(s)} \times 100\%. \tag{1}$$

In equation (1), $\dot{q}(s)$ represents the angular velocity of the line of sight caused by missile body disturbance. $\dot{\vartheta}(s)$ represents the missile body disturbance. In the structure figure, $H(s)$ is the rate gyro transfer function; usually, the guidance signal such as angular velocity of the line of sight can be taken from the angular rate gyro output. According to the structure figure of the pitch-yaw seeker in Figure 1, we can obtain the expanded formula of DRR as follows:

$$\frac{\dot{q}(s)}{\dot{\vartheta}(s)} = \frac{s[K_E K_T H(s) + G_D(s)H(s)(Ls+R)]}{s[Js(Ls+R) + G_D(s)(Ls+R) + K_E K_T + G_2(s)K_T H(s)] + G_1(s)G_2(s)K_T}. \tag{2}$$

The DRR definition formula of the pitch frame is the same as that of the yaw frame in form. Only the related parameters of the pitch frame should be changed into those of the yaw frame.

From the DRR definition formula of the pitch-yaw seeker in equation (2), it can be seen that the main difference between DRR definition of the pitch-yaw seeker and roll-pitch seeker is the different extraction methods of line-of-sight angular velocity $\dot{q}(s)$. The pitch-yaw seeker is a platform seeker that can extract the angular velocity of the line of sight directly from the angular velocity gyro $H(s)$. The roll-pitch seeker is a semistrapdown seeker without angular velocity gyro, so the line-of-sight angular velocity can only be obtained by semistrapdown calculation.

Figure 2 shows the mode of a roll-pitch seeker. The roll-pitch seeker is an infrared seeker with a semistrapdown system. The roll-pitch seeker is composed of detectors and two frames. The frames include an inner frame and an outer frame, among which the roll frame is the outer frame and the pitch frame is the inner frame. The detector is fixed on the missile body, which is used to detect the target and obtain the detector error angles $\varepsilon_p, \varepsilon_y$. The calculation of the error angle of the detector needs the information of target and

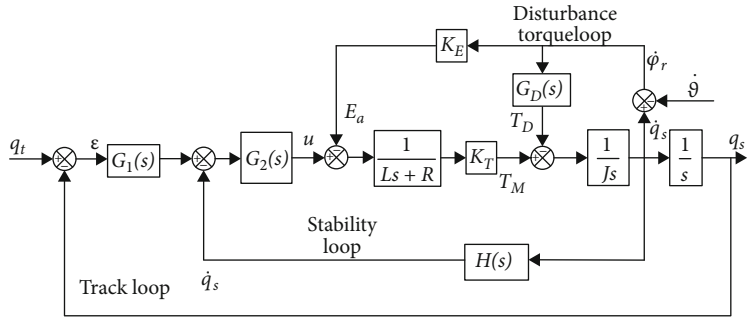

Figure 1: Structure of the pitch-yaw seeker.

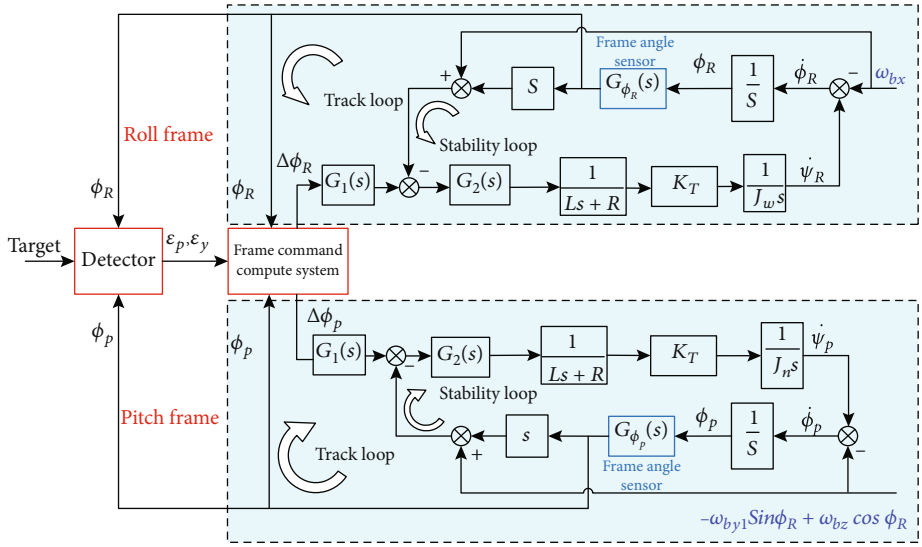

Figure 2: Model of the roll-pitch seeker.

frame angles ϕ_R, ϕ_P. As the input values, the detector error angles can be output as frame angle instruction $\Delta\phi_R, \Delta\phi_P$ after processing by the frame command computing system. The two frames of the roll-pitch seeker will rotate in accordance with the frame angle instruction. During the frame rotation, the frame angle instruction will go through two loops: the stabilization loop and the tracking loop.

The input of the stabilization loop is the rotational angular velocity instruction $\dot{\phi}_{RC}, \dot{\phi}_{PC}$ of the frame relative to the inertial space, which is obtained by differentiator $G_1(s)$. The rotational angular velocity instruction $\dot{\phi}_{RC}, \dot{\phi}_{PC}$ is processed by the voltage sensor $G_2(s)$ and the motor sensors $1/Ls + R$, $1/J_\omega$ and are combined with interference torque $G_D(s)$, counterpotential torque K_E, and other interferences to obtain the current rotational angular velocity ω_{wx}, ω_{nz} of the frame relative to the inertial space. The missile body disturbances on the pitch frame and the roll frame of the roll-pitch seeker are different. For the roll frame, the missile body disturbance is only related to the roll angular velocity of the missile body. For the pitch frame, the body disturbance is related to the pitch angular velocity and yaw angular velocity of the missile body. In addition, since the roll frame is an external frame and the pitch frame is an internal frame, the pitch frame is also affected by the coupling disturbance of the roll frame.

The roll-pitch seeker consists of two frames, the roll frame and pitch frame, so the DRR needs to be defined separately on two loops. Figures 3 and 4 show the structure of the DRR mode of two loops. During the flight of a missile, the disturbances in the three directions of roll, pitch, and yaw of the missile are coupled to the seeker control system through the interference torque loop and the counter electromotive force loop, which affect the motion of the frame and the performance of the seeker control system.

Due to the semistrapdown system of the roll-pitch seeker, the seeker cannot directly measure the rotational angular velocity ω_{wx}, ω_{nz} of the frame relative to the inertial space through the angular velocity gyro. Therefore, we need to obtain the numerical value of the rotational angular velocity through the semistrapdown calculation. The calculation method is as follows. Firstly, the angular velocity of the frame relative to the missile body $\dot{\phi}_R, \dot{\phi}_P$ is calculated from the angular velocity of the frame relative to the inertial space ω_{wx}, ω_{nz} and missile body disturbance. The roll frame is only affected by the body disturbance, so the body disturbance of the roll frame is the rotational velocity of the missile ω_{bx}. The pitch frame is affected by the disturbance of the missile body and the roll frame together, so the disturbance of the

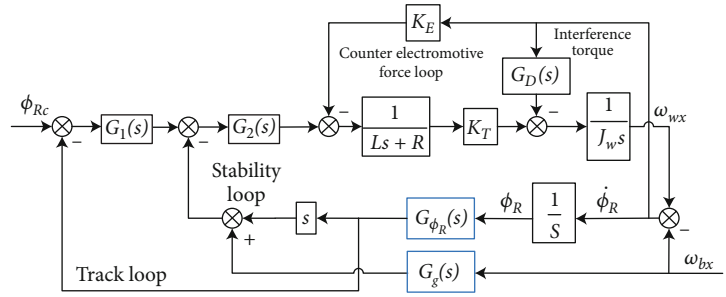

Figure 3: DRR model of the roll loop.

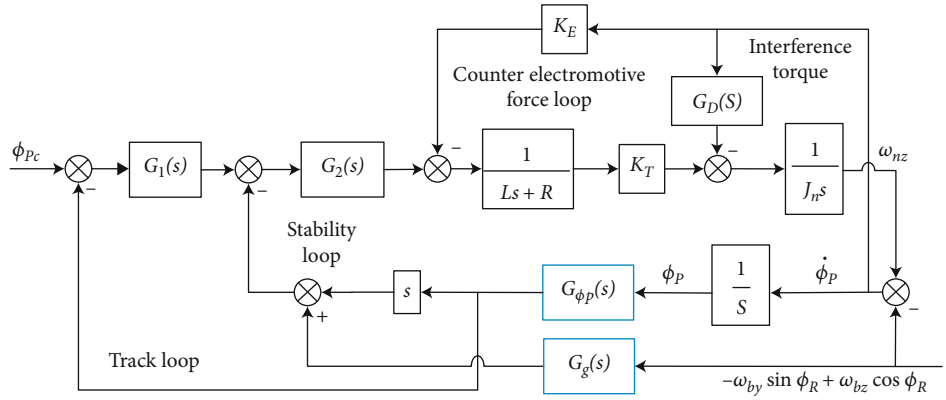

Figure 4: DRR model of the pitch loop.

pitch frame are the pitch, yaw angular velocity of the missile body ω_{by}, ω_{bz}, and the roll frame angle ϕ_R. The rotational angular velocity of the frame relative to the missile body $\dot{\phi}_R$, $\dot{\phi}_P$ can be processed by the integrator, and we can obtain the rotational angle of the frame relative to the missile body ϕ_R, ϕ_P. This information can be measured by the angle sensors $G_{\phi R}(s), G_{\phi p}(s)$ on the seeker. Then, the frame angle information ϕ_R, ϕ_P is processed by the differentiator and combined with the angular velocity of the missile body, and the angular velocity of the frame ω_{wx}, ω_{nz} relative to the inertial space can be calculated.

The frame angular velocity information ω_{wx}, ω_{nz} can be obtained by using this method of semistrapdown calculation. These angular velocity values ω_{wx}, ω_{nz} can be used to define the DRR of the roll-pitch seeker.

The DRR shows the decoupling ability of the seeker, which is also known as the decoupling precision. DRR is an important index to measure the performance of the seeker. DRR is usually defined as the ratio of rotational angular velocity of the platform relative to the inertial space caused by projectile body disturbance and the angular velocity of missile body disturbance.

For the traditional pitch-yaw seeker, the pitch frame and yaw frame can be designed separately when the roll disturbance of the missile body is ignored. The pitch frame can isolate the disturbance of the missile body's pitch direction, and the yaw frame can isolate the disturbance of the missile body's yaw direction. For the roll-pitch seeker, its roll frame can isolate the missile body's roll motion. The DRR of the roll frame is defined as

$$R_x = \frac{\omega_{wx}}{\omega_{bx}} \times 100\%, \tag{3}$$

where R_x is the DRR of the roll frame and ω_{wx} is the rotational angular velocity of the outer frame relative to the inertial space caused by the roll disturbance of the missile body ω_{bx}.

The control frame of the seeker generally consists of four loops: the stability loop, the track loop, the interfering torque loop, and the counter electromotive force loop. The stability loop and the track loop are the basic loops of the seeker control system, which ensure the stability of the frame and the tracking of the target. The interference torque loop and the counter electromotive force loop are the interference loops in the seeker control system. The interference torque loop acts on the motor load to produce the interference torque. The interference torque is related to the interference torque model $G_D(s)$ and the frame angular velocity $\dot{\phi}_R$. The counter electromotive force circuit acts on the motor armature to produce the reverse armature voltage, which is related to the coefficient of the reverse electromotive force K_E and the angular velocity of the frame $\dot{\phi}_R$. The missile body disturbance acts on the seeker control system through the interference torque loop and the counter electromotive force loop and generates uncertain disturbance in the whole loop, which reduces the tracking accuracy of the platform. According to the block diagram, without considering the missile body

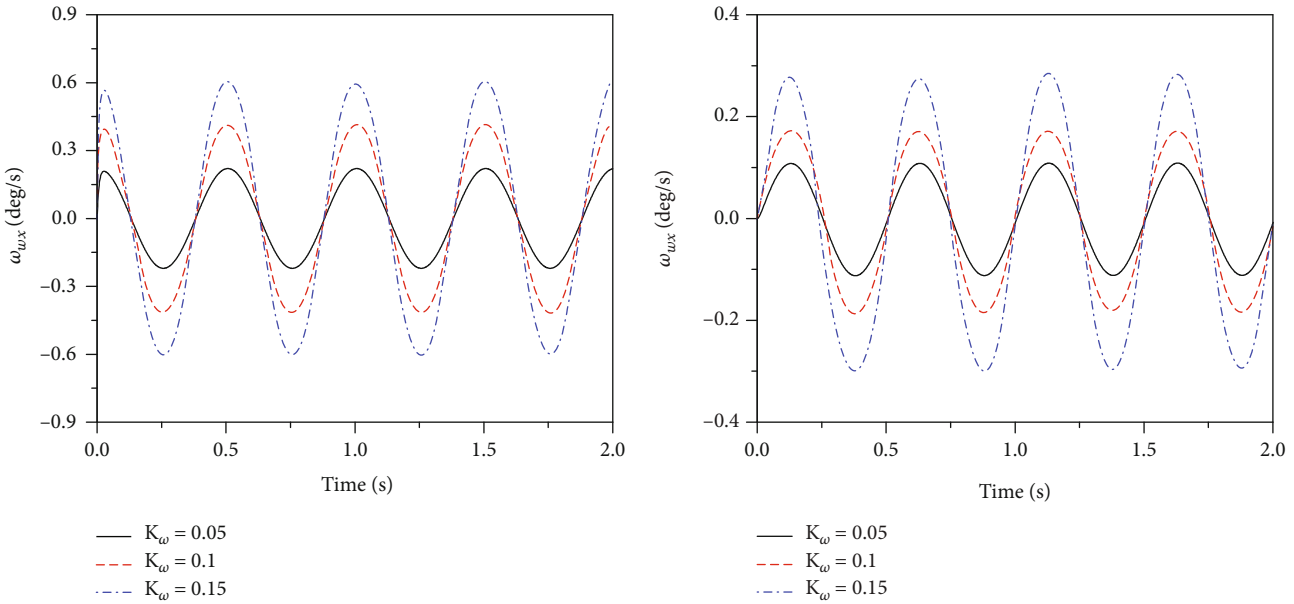

(a) Viscous damping torque

(b) Spring torque

Figure 5: DRR of the roll interference torque.

angular rate gyro and the frame angle sensor, it can be deduced that the DRR of the roll frame is

$$R_x = \frac{G_D(s)(Ls+R) + K_T K_E}{J_w L s^2 + (J_w R + G_D(s)L)s + G_2(s)K_T + K_T K_E}. \quad (4)$$

It can be seen from equation (4) that since the counter electromotive force coefficients K_E and $G_D(s)$ are small, increasing the amplitude gain of the stability loop can improve the DRR of the frame. The interference torques that affect the DRR mainly include spring torques and viscous damping torques. The spring torque coefficient is K_n, and the viscous damping torque coefficient is K_ω, which are proportional to the spring torques and viscous damping torques, respectively. The DRR formula of the difference torque can be obtained by substituting (4), respectively, with the viscous damping torque model $G_D(s) = K_\omega$ and the spring torque model $G_D(s) = K_n/s$.

$$R_x^\omega = \frac{K_\omega(Ls+R) + K_T K_E}{J_w L s^2 + (J_w R + K_\omega L)s + G_2(s)K_T + K_T K_E},$$
$$R_x^s = \frac{(K_n L + K_T K_E)s + K_n R}{J_w L s^3 + J_w R s^2 + (K_n L + G_2(s)K_T + K_T K_E)s}. \quad (5)$$

The DRR caused by the interference torque is related to the kind and coefficient of the interference torque. Refer to the frame parameters of the seeker in Reference [15], as well as the selection of the viscous damping torque coefficient and spring torque coefficient, sine wave with amplitude of 5°/s and frequency of 2Hz is selected as the roll frame input of the missile body disturbance. The roll angular velocity under the action of the single interference torque is shown in Figure 5.

The pitch frame can isolate the components of the missile body's pitch direction and yaw direction disturbance in the motion direction of the pitching frame. The projection of the missile body's disturbance angular velocity in the z direction of the pitching frame is $\omega_{dz} = -\omega_{by} \sin\phi_R + \omega_{bz} \cos\phi_R$, and the DRR of the pitching frame is defined as

$$R_z = \frac{\omega_{nz}}{\omega_{dz}} = \frac{\omega_{nz}}{-\omega_{by} \sin\phi_R + \omega_{bz} \cos\phi_R} \times 100\%, \quad (6)$$

where R_z is the DRR of the pitching frame and ω_{nz} is the rotational angular velocity of the inner frame relative to the inertial space caused by the projectile body pitching and yaw disturbance. The DRR model of the pitch frame is the same as that of the roll frame. When the rolling frame angle is 0, the pitch frame can only isolate the missile body from the pitch direction disturbance.

The pitch frame and roll frame have the same DRR function:

$$R_z = \frac{G_D(s)(Ls+R) + K_T K_E}{J_w L s^2 + (J_w R + G_D(s)L)s + G_2(s)K_T + K_T K_E}. \quad (7)$$

Refer to the frame parameters of the seeker in Reference [15], as well as the selection of the viscous damping torque coefficient and spring torque coefficient, sine wave with amplitude of 5°/s and frequency of 2Hz is selected as the pitch frame input of the missile body disturbance. The pitch angular velocity under the action of the single interference torque is shown in Figure 6.

From Figures 5 and 6, we can find that roll loop and pitch loop performance will be influenced by the action of a missile disturbance in different torque types and

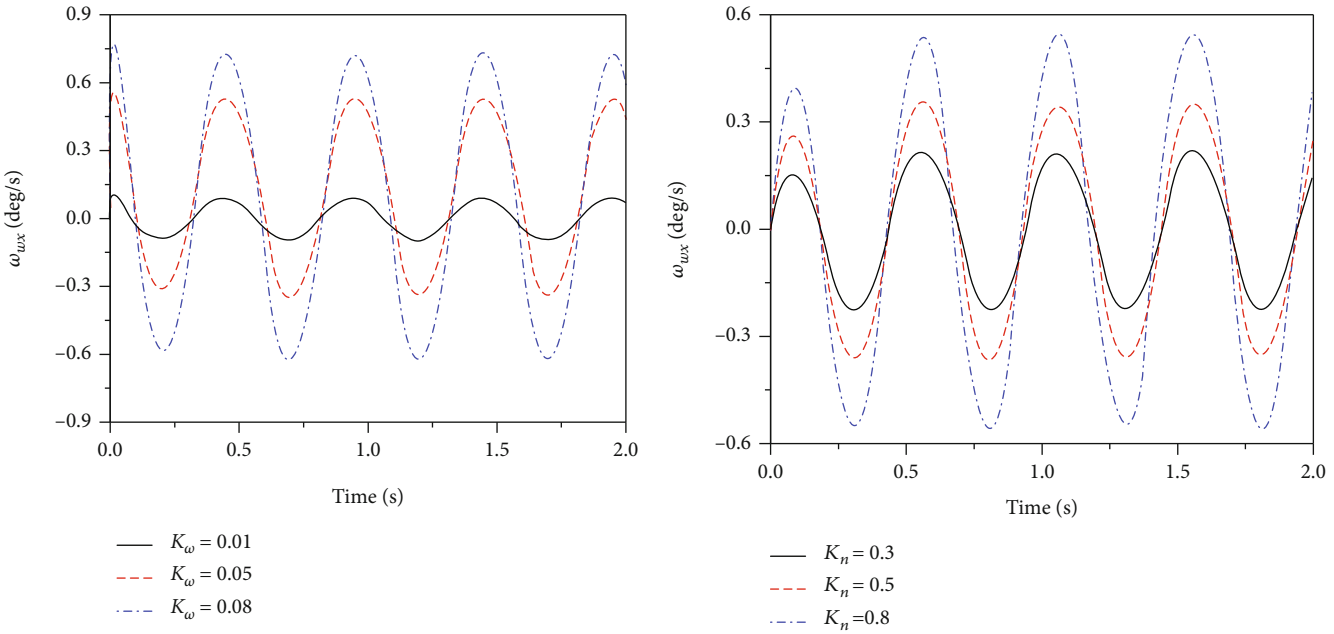

(a) Viscous damping torque

(b) Spring torque

Figure 6: DRR of the pitch interference torque.

different torque coefficients. It is necessary to choose the right method on DRR compensation to eliminate the adverse effects on the performance of seeker guidance control.

3. DRR Compensation Method Based on ESO

The state observer can reconstruct the system state based on the known input and measurement output of the system. The extended state observer (ESO), which is based on the nonsmooth continuous output error correction, is suitable for the uncertain object of the observer. ESO can output the expanded state of the system, and the expansion of the state can estimate system disturbance, which includes the inside and outside disturbances. The expansion of the state feedback control obtained by ESO can effectively restrain the influence of various disturbances on the system, to improve the anti-interference ability of the system. The extended state observer considers the imprecise fuzzy object and external disturbance of the system model as the system disturbance to estimate and compensate for. The automatic estimation and compensation of disturbance are the most important part in the controller design.

3.1. Mathematical Derivation of the ESO Structure. The input quantity of the extended state observer is the output and control quantity of the control object, and there is no requirement to describe the transfer relation function of the object, so the mathematical model of the controlled object is unnecessary. Its output is the estimation of each order quantity of the system, as well as the disturbance of the system. The extended state observer unifies the deterministic and uncertain disturbances of the system into a "summation disturbance" and performs real-time estimation. With the control law, the estimated disturbances are compensated to eliminate the influence of the internal and external disturbances of the system.

Assume the n-order nonlinear system under the action of unknown external disturbance is

$$x^{(n)} = f\left(x, \dot{x}, \cdots, x^{(n-1)}, t + w(t)\right) + bu(t), \tag{8}$$

where $f(x, \dot{x}, \cdots, x^{(n-1)}, t + w(t))$ is the unknown uncertain function, $w(t)$ is the unknown external disturbance, $u(t)$ is the control quantity, and b is the control coefficient. The measured output is $y(t) = x(t)$. The extended state observer depends on the control quantity $u(t)$ and the measured values $y(t)$ and reconstructs the state of the system $\dot{x}, \cdots, x^{(n-1)}$. Uncertainties and disturbances $a(t) = f(x, \dot{x}, \cdots, x^{(n-1)}, t + w(t))$ will be expanded into the state of the system x_{n+1}, and formula (8) can be written as

$$\begin{cases} \dot{x}_1 = x_2, \\ \dot{x}_2 = x_3, \\ \quad \vdots \\ \dot{x}_n = x_{n+1} + bu, \\ \dot{x}_{n+1} = -\omega(t). \end{cases} \tag{9}$$

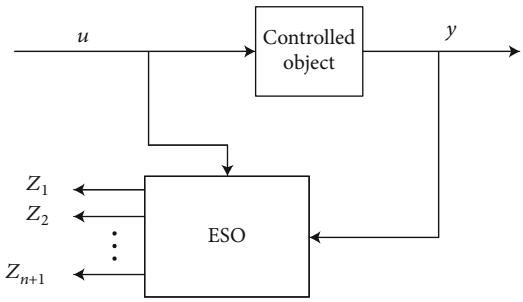

Figure 7: Model of the ESO.

Design ESO which is used in formula (9):

$$\begin{cases} \dot{z}_1 = z_2 - \beta_1 g_1(e), \\ \dot{z}_2 = z_3 - \beta_2 g_2(e), \\ \quad \vdots \qquad\qquad e = z_1 - y, \beta_i > 0, i = 1, 2, \cdots, n, \\ \dot{z}_n = z_{n+1} - \beta_n g_n(e) + bu, \\ \dot{z}_{n+1} = -\beta_{n+1} g_{n+1}(e), \end{cases} \tag{10}$$

where β_i is an adjustable parameter and $g_i(e)$ is the constructed nonlinear continuous function. They satisfy $eg_i(e) > 0$, $\forall e \neq 0$, $g_i(0) = 0$.

By selecting the appropriate parameters β_i, the extended state observer (10) can estimate the state variables of the system $x_1(t), x_2(t), \cdots, x_n(t)$ and the real-time action of the extended state $x_{n+1}(t)$: $z_1(t) \to x_1(t), z_2(t) \to x_2(t), \cdots, z_n(t) \to x_n(t), z_{n+1}(t) \to x_{n+1}(t)$.

The structure of the extended state observer is shown in Figure 7.

It is now possible to estimate the summation disturbance by using the state estimator. To this end, consider a nonlinear observer of the form:

$$\begin{cases} \dot{z}_1 = z_2 - \dfrac{\beta_1}{\varepsilon} |e_1|^{\alpha_1} \operatorname{sign}(e_1) + ku, \\ \dot{z}_2 = -\dfrac{\beta_2}{\varepsilon^2} |e_1|^{\alpha_2} \operatorname{sign}(e_1), \end{cases} \qquad e = z_1 - y, \beta_i > 0, i = 1, 2, \cdots, n, \tag{11}$$

where $\alpha_2 = \alpha \in (0, 1)$, $\alpha_1 = 2\alpha_2 + 1/3$, and $\varepsilon \in (0, 1)$. α_1 and α_2 and β_1 and β_2 are system parameters of ESO. We can prove the stability of formula (11) with the following process.

Suppose $e_1 = z_1 - y$, $e_2 = z_2 + \omega_x$ stand for the estimation errors. Considering the extended system (10) and observer system (11) and that $L > 0, \sigma = 1 - \gamma/\gamma$ exists, $\gamma \in (0, 1/2)$ makes the estimation errors be stabilized in the following internals with finite time, as shown below:

$$\begin{cases} |z_1 - y| \le L\varepsilon^{3\sigma}, \\ |z_2 - x_2| \le L\varepsilon^{3\sigma-1}. \end{cases} \tag{12}$$

The error equations between the extended system (see equation (10)) and the observer system (see equation (11)) can be obtained as

$$\begin{cases} \dot{e}_1 = e_2 - \dfrac{\beta_1 |e_1|^{\alpha_1} \operatorname{sign}(e_1)}{\varepsilon}, \\ \dot{e}_2 = -\dfrac{\beta_2 |e_1|^{\alpha_2} \operatorname{sign}(e_1)}{\varepsilon^2} - \omega(t). \end{cases} \tag{13}$$

Then, considering the following coordinate transformation,

$$\begin{cases} \tau = \dfrac{t}{\varepsilon}, \\ \omega_i(\tau) = \varepsilon_{i-1} e_i(t), i = 1, 2, \end{cases} \tag{14}$$

By ignoring the small quantities, equation (13) can be written as follows:

$$\begin{cases} \dfrac{d\omega_1}{d\tau} = \omega_2 - \beta_1 |\omega_1|^{\alpha_1} \operatorname{sign}(\omega_1), \\ \dfrac{d\omega_2}{d\tau} = -\beta_2 |\omega_1|^{\alpha_2} \operatorname{sign}(\omega_1). \end{cases} \tag{15}$$

Definition 1 (see [27–29]). Let $f(x) = [f_1(x), \cdots, f_n(x)]^T : R^n \to R^n$ be a vector field. This vector field satisfies that $\forall \varepsilon > 0$, $(r_1, \cdots, r_n) \in R^n$ exists, where $r_i > 0, i = 1, 2, \cdots, n$, and

$$f_i(\varepsilon^{r_1} x_1 \cdots \varepsilon^{r_n} x_n) = \varepsilon^{k+r_i} f_i(x), i = 1, 2, \cdots n. \tag{16}$$

According to Definition 1, let $f_\omega(c^{r_1}\omega_1, \varepsilon^{r_2} x_2)$ stand for the vector function of the system (15). There exists

$$\begin{aligned} f_\omega(c^{r_1}\omega_1, \varepsilon^{r_2} x_2) &= \begin{pmatrix} c^{r_2}\omega_2 - \beta_1 c^{r_1} |\omega_1|^{\alpha_1} \operatorname{sign}(\omega_1) \\ -\beta_2 c^{r_1} |\omega_1|^{\alpha_2} \operatorname{sign}(\omega_1) \end{pmatrix} \\ &= \begin{bmatrix} c^{r_1+m} & 0 \\ 0 & c^{r_2+m} \end{bmatrix} \begin{pmatrix} \omega_2 - \beta_1 |\omega_1|^{\alpha_1} \operatorname{sign}(\omega_1) \\ -\beta_2 |\omega_1|^{\alpha_2} \operatorname{sign}(\omega_1) \end{pmatrix}. \end{aligned} \tag{17}$$

Definition 2 (see [27–29]). In the finite time stability, for nonlinear systems, $\dot{x} = f(x), f(0) = 0, x \in R^n$. If and only if the system is Lyapunov stable and converges in finite time, the equilibrium point of the system $x = 0$ is stable in finite time.

Lemma 3 (see [30]). *Suppose the vector field $f(x)$ is homogeneous with degree m with respect to ν. Then, the origin is a finite-time-stable equilibrium under $f(x)$ if and only if the origin is an asymptotically stable equilibrium under $f(x) < 0, m < 0$.*

Lemma 4 (see [30]). *For any continuous function $g(t)$ and $|g(t)| < \delta_0$ and considering the following disturbed system,*

$$\dot{x} = f(x, t) + g(t). \tag{18}$$

If there is a C^1 smooth positive definite function $V(x)$ and for any $\beta_1 > 0$, $\beta_2 \in (0, 0.5)$, which satisfies

$$\dot{V}(x) + \beta_1 V^{\beta_2}(x) \leq 0. \tag{19}$$

So there exist $L_0 > 0$, $\gamma_0 \in (0, 05)$, and a finite adjustment time T_{reach}, and then, the solution of the system (18) satisfies

$$\|x\| \leq L_0 \delta_0{}^{\sigma_0}, \quad \sigma_0 = \frac{(1-\gamma_0)}{\gamma_0}. \tag{20}$$

In addition, according to the Routh stability criterion, $k_2 s_2 + k_1 s + k_0$ is the Hurwitz polynomial. The origin of the system (15) is the equilibrium point of asymptotic stability because of the linear correlation between the vector field f_ω and polynomial $k_2 s_2 + k_1 s + k_0$. According to Lemma 3, the origin of the system (15) is finite-time stable. Next, by using Lemma 4, in which there is a positive number μ, this makes the solution of the system (15) satisfy $|w(\tau)| \leq \mu(w_0 \varepsilon^2)^\sigma$ in finite time. Finally, according to equation (14), it can be observed that the estimation errors are able to meet $|e_i| \leq \|w(\tau)\| \varepsilon^{-i+1} = L\varepsilon^{3\sigma - i + 1}$, where $L = \mu w_0^\sigma$, thus completing the stability proof.

For the nonlinear system formula (11), the extended state observer is used to estimate the total disturbance of the system and compensate for it, which can make the nonlinear system become a linear control system, thus eliminating the uncertainty and nonlinear influence in the system, making the system have strong anti-interference ability and improving the control accuracy of the system.

The structure of the ESO compensation loop of the roll frame is shown in Figure 8, and the structure of the ESO loop of the pitch frame is shown in Figure 9.

3.2. Compensation Method Based on ESO and Comparisons between Methods

3.2.1. ESO-Based Method Compared with the Kalman Filtering Method. Design compensation strategies for the roll frame and pitch frame, respectively, and simulate the DRR of the frame before and after compensation. The random error signal with mean value of 0 and variance of 0.1 deg is selected as the seeker detector noise. Different interference torques are selected as the environment variables, and the effect of the DRR compensation strategy based on ESO is simulated and compared with that of the Kalman filtering compensation method. Figure 10 shows the simulation results of roll frame angular velocity by the use of the DRR compensation strategy and Kalman filtering compensation method with a large filtering error. Figure 11 shows the simulation results of roll and pitch frame angular velocity by the use of the DRR compensation strategy and Kalman filtering compensation method under combined torque interference.

Due to the influence of various interfering torques, the guidance information such as line-of-sight angular velocity output of the roll-pitch seeker will have errors. It is a useful way to deal with this kind of problems to estimate and compensate for the error caused by various interferences through appropriate estimation methods. As a widely used filtering estimation method, the Kalman filter method can be used to estimate the amount of interference. As an optimal estimation method, Kalman filtering needs to establish complete state equations and measurement equations to optimize the estimated state variables gradually. Therefore, whether the established state equation can reflect the real physical meaning of state variables and whether the measurement equation and measurements are accurate will affect the filtering estimation effect of the Kalman filter.

For the roll-pitch seeker, the Kalman filter equation is established to estimate the disturbance quantity. The angle of the line of sight, angular velocity of the line of sight, the angular acceleration, and the disturbance angular acceleration are taken as the state quantities. Angular velocity of the line of sight is generally used as the measurement of the Kalman filter equation. Since the roll-pitch seeker cannot directly obtain angular velocity, which needs to be obtained by semistrapdown calculation. Therefore, the accuracy of angular velocity obtained by the line of sight will have a direct impact on the accuracy of the Kalman filter measurement equation.

The Kalman filter estimation method is very effective for the pitch-yaw seeker, which can directly obtain the accurate angular velocity of the line of sight, but for the roll-pitch seeker, there is an error risk when using the Kalman filter method. The ESO-based method will not be affected by the angular velocity error of the line of sight, so when the filtering error is large, the estimation compensation effect of the ESO-based method will be better than that of the Kalman filtering method. It can be used in the roll-pitch seeker system, which is the superiority of the ESO-based method over the Kalman filtering method. The simulation results in Figures 10 and 11 can also illustrate this conclusion.

From Figure 10, the amplitude of the angular velocity of the roll frame motion under the action of the disturbance torque is greatly reduced by the estimation and compensation of the disturbance by the expanded state observer, which can well isolate the influence of the projectile body disturbance on the roll frame motion. For viscous damping moment, the noise of the seeker detector has a deep influence on the compensation effect. For spring torque, the influence is not deep. From the simulation, we know that the compensation result of the Kalman filtering method may be affected by the filtering precision, and the compensation effect is worse than that of the DRR compensation method based on ESO when the filtering error is large.

From Figure 11, the DRR generated by the combined interference torque is relatively large. After ESO compensation, the DRR of the roll frame and the pitch frame are all reduced greatly. Each of the reduction is an order of magnitude reduction and significantly improves the seeker's ability to isolate missile body disturbance. From the simulation, we also know that the compensation effect of the Kalman filtering compensation method is worse than that of the DRR compensation method based on ESO when the filtering error is large.

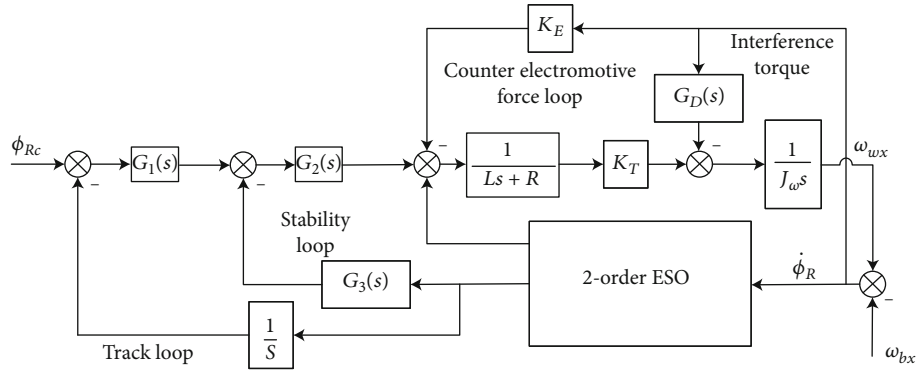

Figure 8: ESO model of the roll frame.

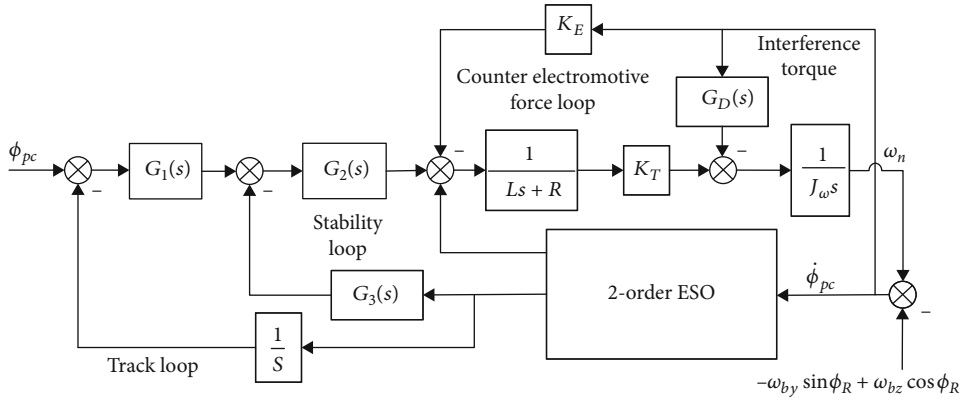

Figure 9: ESO model of the pitch frame.

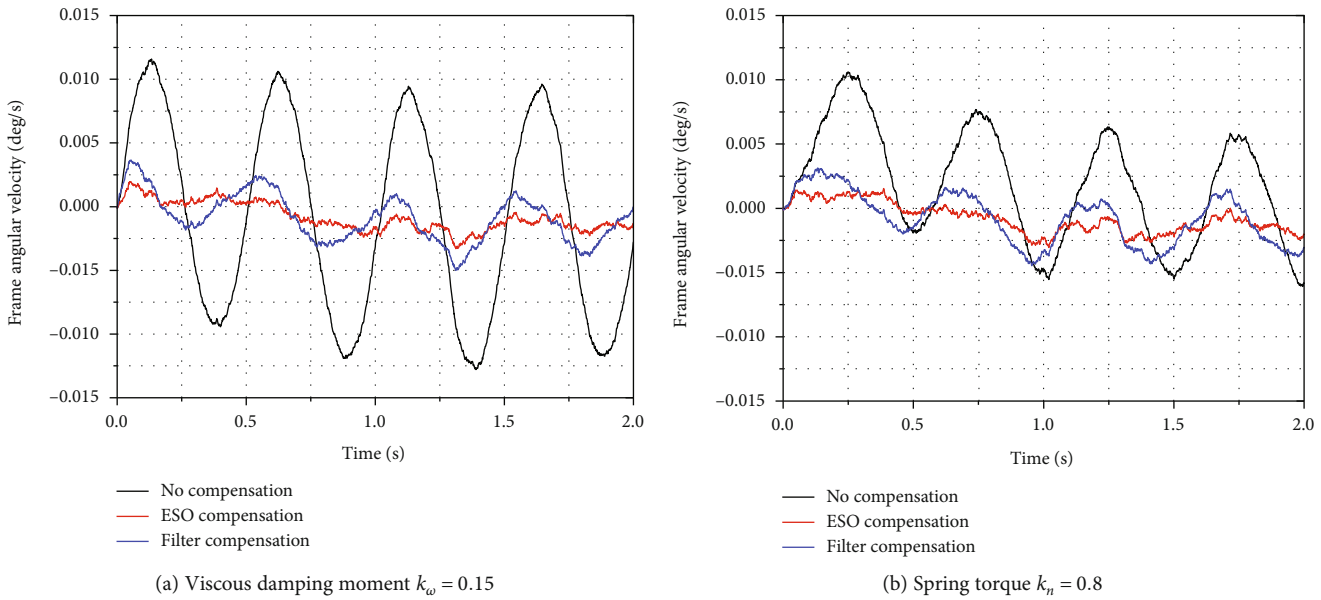

(a) Viscous damping moment $k_\omega = 0.15$

(b) Spring torque $k_n = 0.8$

Figure 10: Angular velocity of the roll frame under interference torque after ESO compensation.

3.2.2. ESO-Based Method Compared with the Differentiator Method. From Figures 8 and 9, we know that as the input of ESO, the angular velocity of the frame can only be obtained by semistrapdown calculation. Therefore, the error caused by the semistrapdown calculation will result in a deviation between the real frame angular velocity ω_{wx} and the ESO input. This deviation $\Delta\omega_{wx}$ will adversely affect the effect of DRR compensation. In the case of input information error $\Delta\omega_{wx}$, the compensation effect of the existing differentiator compensation methods will be adversely affected. Figure 12

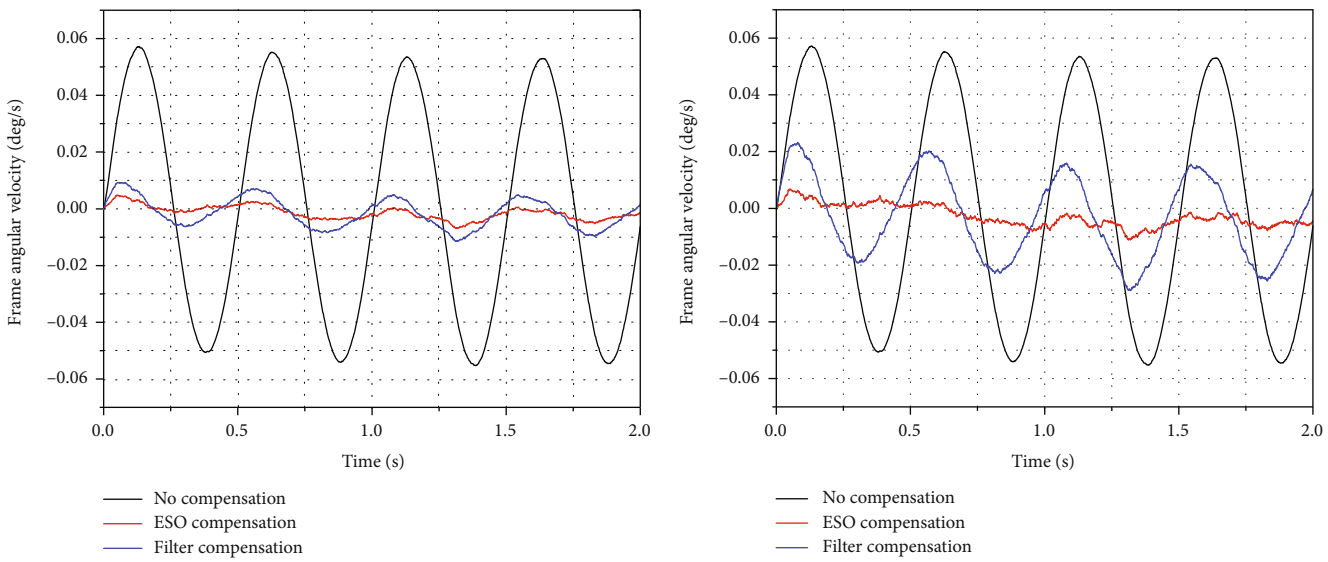

(a) Combined torque interference for the roll frame

(b) Combined torque interference for the pitch frame

Figure 11: Angular velocity under combined torque interference after ESO compensation with $k_\omega = 0.15$ and $k_n = 0.8$.

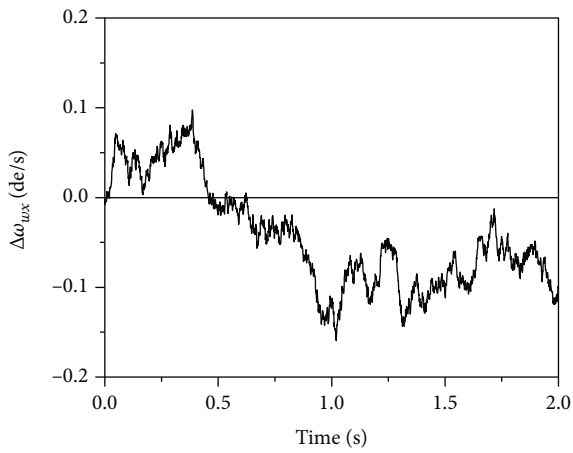

Figure 12: Angular velocity deviation caused by semistrapdown calculation.

shows the angular velocity deviation caused by semistrapdown calculation. Figure 13 shows the effect of DRR compensation based on ESO with the angular velocity deviation, which is compared with that of the differentiator compensation method.

From Figure 13, we know that when there is input information error, the effect of the compensation method based on the differentiator will be affected by the error information. If the angular velocity obtained through semistrapdown calculation is inaccurate, it is difficult to eliminate its influence on the frame motion through the differentiator. The effect of compensation based on ESO will be less affected by the error information. By estimating and compensating the disturbance in the stable loop through ESO, the capability of the seeker frame to isolate the missile body disturbance can be improved with at least one order of magnitude, and the missile body disturbance can be significantly inhibited.

3.2.3. ESO-Based Method Compared with the Feedforward Method. Figure 14 shows the DRR compensation simulation for the real and inaccurate roll-pitch seeker model, respectively. Select typical simulation parameters: the roll disturbance of the missile body is sinusoidal motion with amplitude 5°/s and frequency of 2 Hz. $k_\omega = 0.15$ and $k_n = 0.8$. From the simulation results shown in Figure 14, we know that when the feedforward compensation method is adopted to compensate for DRR of the real roll-pitch seeker model, feedforward compensation can well isolate the missile body disturbance, and the ESO compensation method can have a good compensation effect too. When there is an error between the current roll-pitch seeker model and the real roll-pitch seeker model, the compensation effect of the feedforward compensation method is reduced, while the ESO compensation method still has a good compensation effect. The compensation effect of the feedforward compensation method depends on the model selected at the time of design. When the model has deviation, its ability to isolate the missile body disturbance decreases. However, the ESO compensation method does not depend on the model adopted at the time of design and can achieve a better compensation effect under different conditions.

3.3. The Influence of Frequency Bandwidth on Compensation Effect. The width of the frequency band is also an important loop parameter of the roll-pitch seeker. Increasing the frequency bandwidth of the stability loop can improve the disturbance isolation capability of the missile body of the system [31, 32]. However, due to hardware limitations such as the torque motor and frame angle sensor, the frequency bandwidth of the stability loop cannot be designed to be infinite, and the frequency band is generally 15 ~ 30Hz [33, 34].

In this frequency bandwidth range, the numerical values of frame angular velocity after using the ESO-based DRR

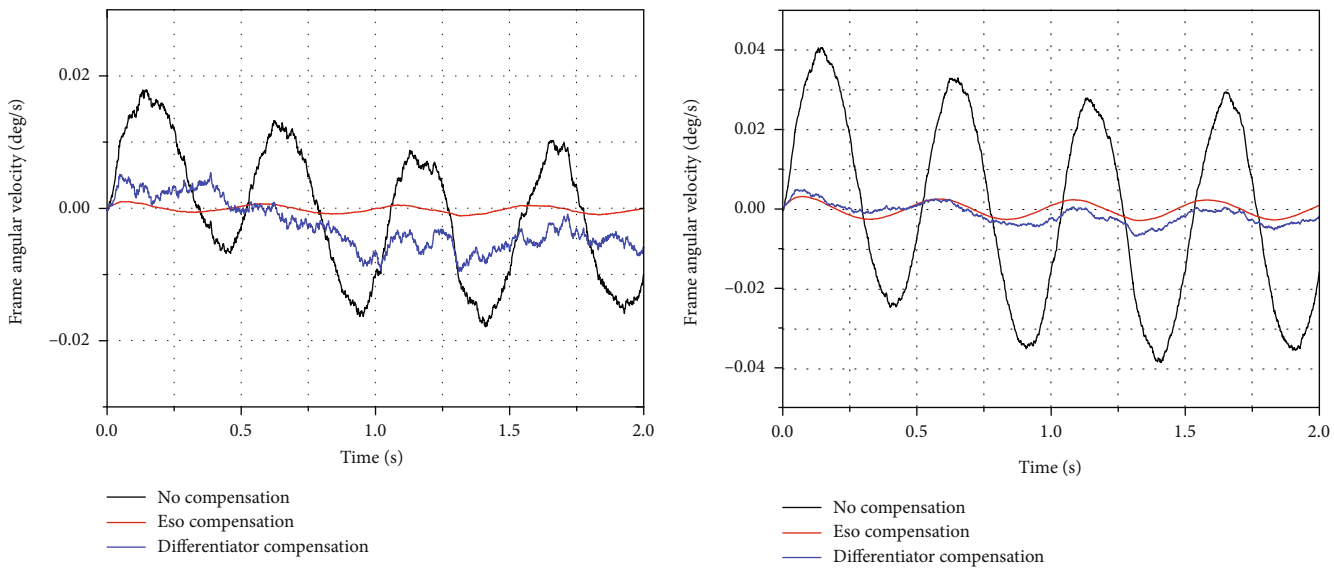

(a) Compensation effect for the roll frame with deviation

(b) Compensation effect for the pitch frame with deviation

Figure 13: Angular velocity of the frame under interference torque with $k_\omega = 0.15$ and $k_n = 0.8$.

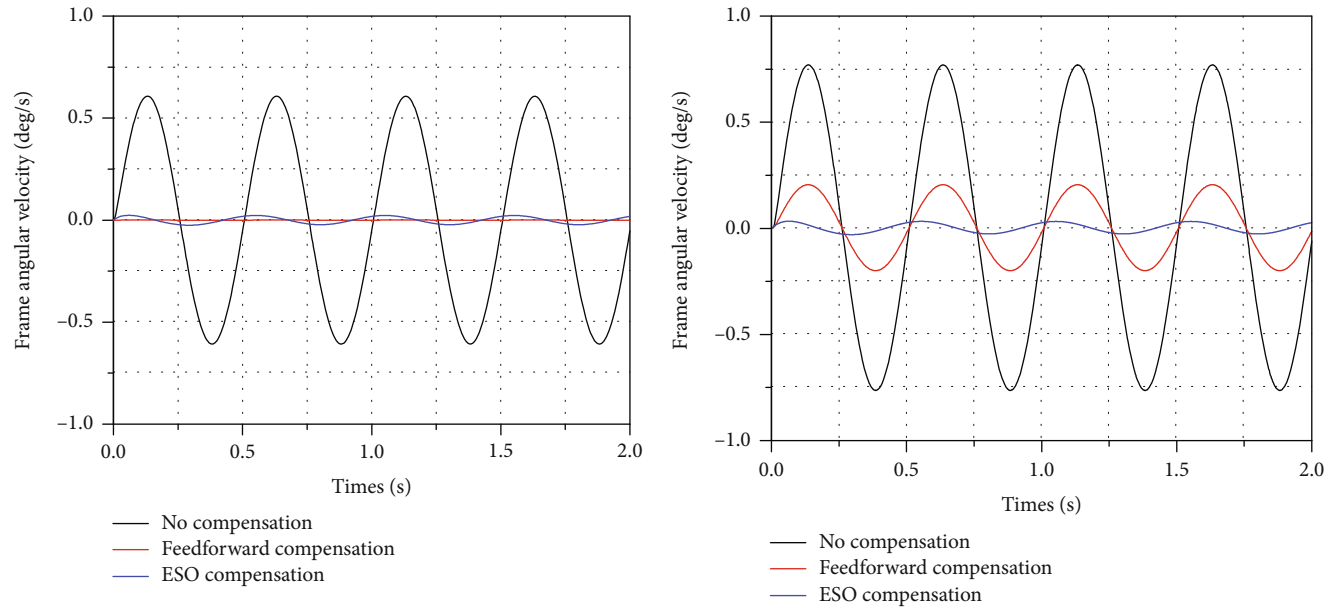

(a) Compensation effect for the real model

(b) Compensation effect for the inaccurate model

Figure 14: Angular velocity of the roll frame by the use of ESO compensation and feedforward compensation.

compensation method with different seeker frequency bandwidths and interference torques are compared by simulation. Referring to model data of the typical roll-pitch seeker in the laboratory, we can set the simulation conditions as shown in Table 1.

From Figure 15, we can know that under different types of interference torques, the frame angular velocity after using the ESO-based DRR compensation method is reduced by an order of magnitude compared with that before compensation. The compensation effects are different with different frequency bandwidths. Four simulation conditions (15 Hz, 20 Hz, 25 Hz, and 30 Hz) are selected. The simulation results

Table 1: Simulation parameters.

Parameters	Values
J_n (kg·m)	0.00305
J_w (kg·m)	0.0087
K_e	(0.5, 0.6, 0.7, 0.8, 0.9, 1.0)
K_ω	(0.05, 0.1, 0.15, 0.2, 0.25, 0.3)
K_n	(0.5, 0.6, 0.7, 0.8, 0.9, 1.0)
ω (Hz)	(15,20,25,30)
deltaT (°/s)	5

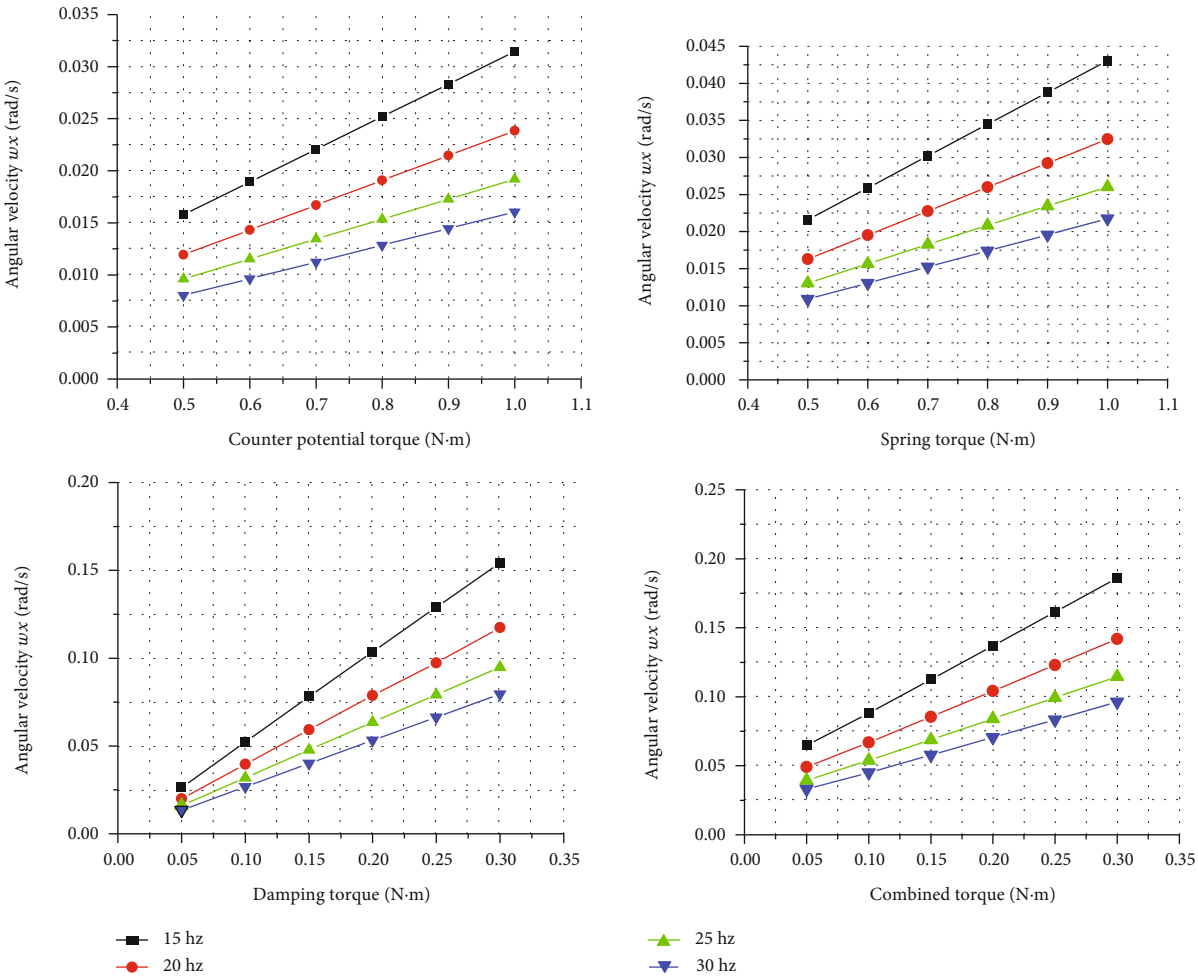

Figure 15: Angular velocity of the frame with different frequency bands after ESO compensation.

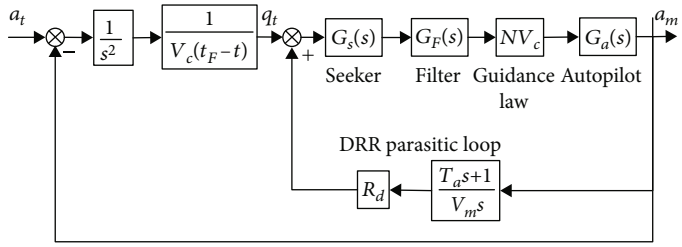

Figure 16: The guidance system model of the roll-pitch seeker.

show that the higher the frequency bandwidth is, the better the compensation effect will be.

In addition, the frame angular velocity after compensation is proportional to the interference torque. The larger the interference torque is, the larger the compensated frame angular velocity will be. The relationship between these two parameters is approximately linear.

4. Analysis of Dimensionless Miss Distance with the ESO Method

For the roll-pitch seeker, since the scale deviation between the detector, the frame angle sensor, and the angular rate gyro can be converted into the scale deviation between the detector and the angular rate gyro R_s and the scale deviation between the frame angle sensor and the angular rate gyro R_m,

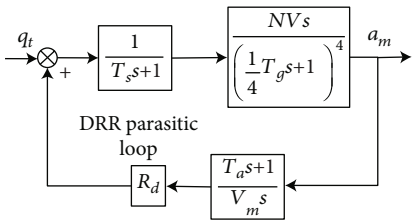

Figure 17: Frame of the parasitic loop of the inverted roll seeker.

Table 2: Simulation parameters.

Parameters	Physical meaning	Values
T_g	Guidance time constant	1
N	Proportional guidance law coefficient	3
$\frac{V_c}{V_m}$	The ratio of relative velocity to projectile velocity	600/400
T_α	Time constant of angle of attack	3
R_d	DRR coefficient	{0.01, 0.04, 0.06, 0.08}
T_F	Terminal guidance time constant	10
T_1	Detector time constant	0.01
T_2	Instruction time constant	0.01
T_3	Line-of-sight angle extraction time constant	0.01
k_1	Tracking loop coefficient	1
k_2	Stability loop coefficient	1

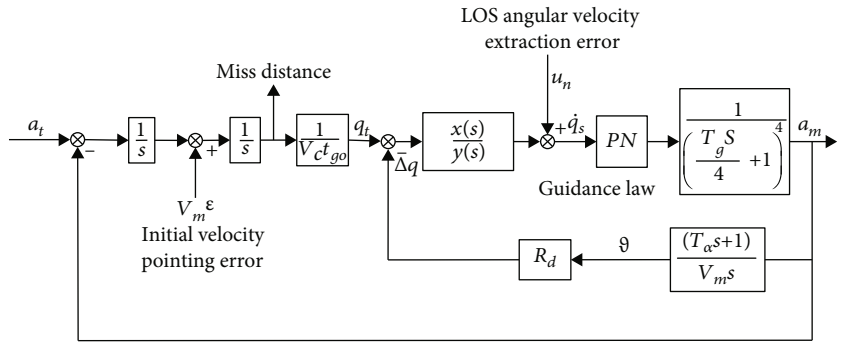

(a) Guidance control system of the roll-pitch seeker without target maneuvering

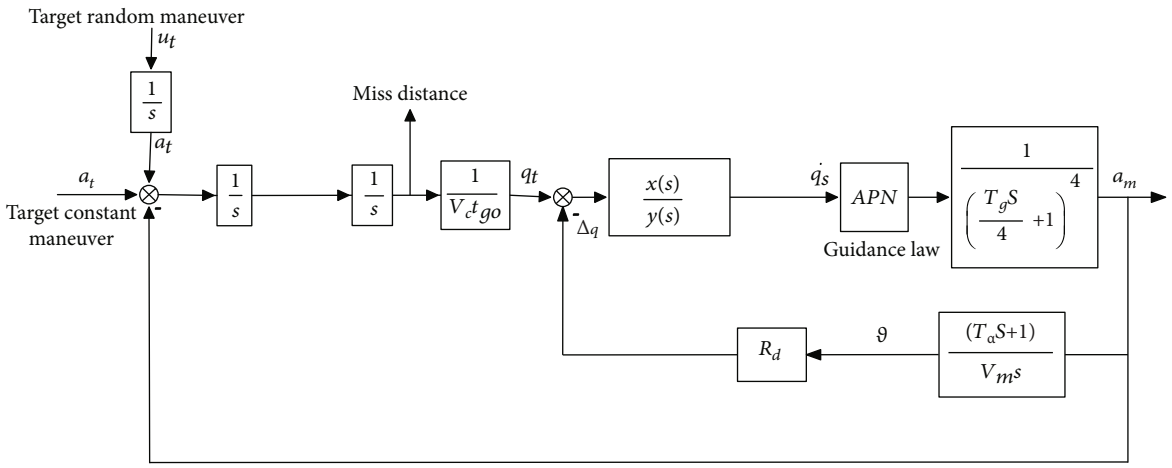

(b) Guidance control system of the roll-pitch seeker with target maneuvering

Figure 18: Guidance control system of the roll-pitch seeker considering typical error sources.

the DRR of the guidance system can be defined as

$$R_d = \frac{\Delta \dot{q}(s)}{\dot{\vartheta}} = (R_s + R_m) \times 100\%. \quad (21)$$

The isolation of the guidance system depends on the symbol and size of the scale deviation sum. With the development of inertial devices, the angular rate gyro scale coefficient k_g in the missile-borne high-precision navigation system has a small fluctuation range, which is within the range of the 1×10^{-4} missile in flight. The scale coefficient of the detector and the scale coefficient of the frame angle sensor can be calibrated and corrected when the seeker is delivered, but the scale coefficient changes during long-term storage and in

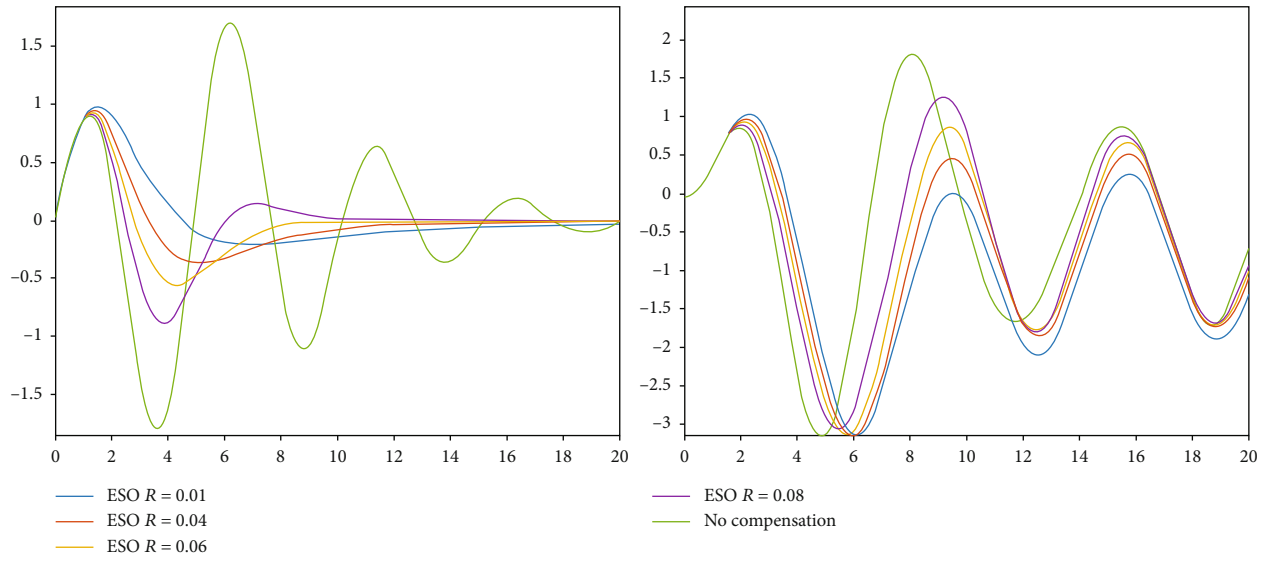

Figure 19: Effect of initial pointing error on dimensionless miss distance under step and wave disturbance.

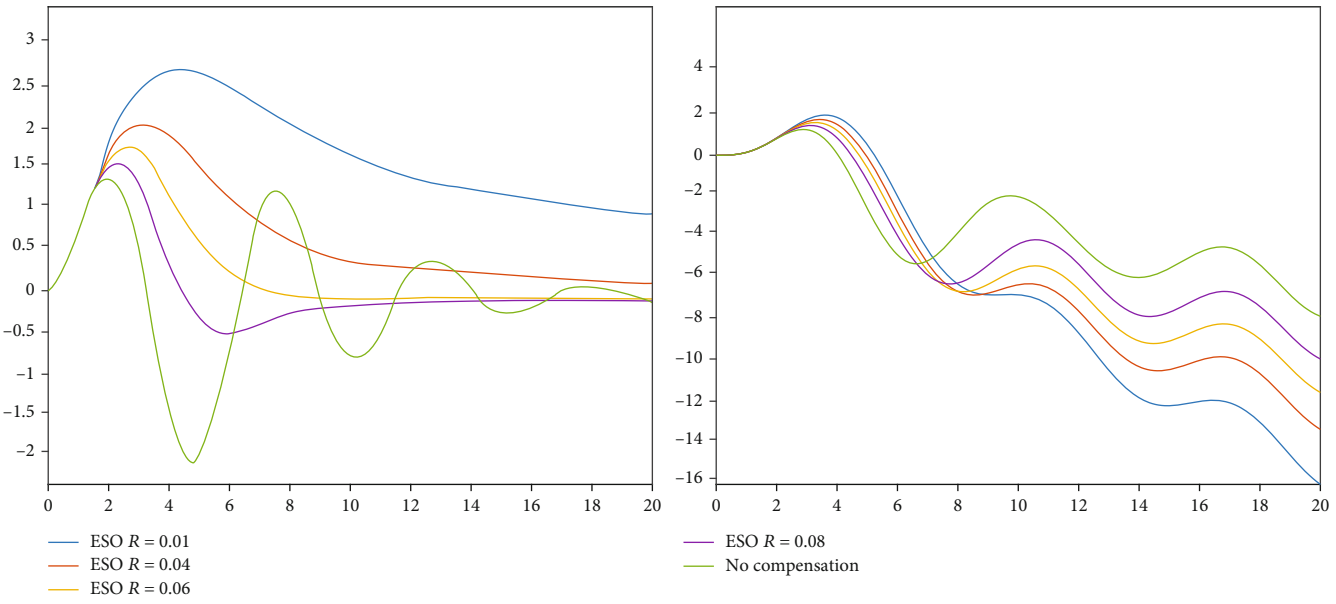

Figure 20: Effect of target constant maneuver on dimensionless miss distance under step and wave disturbance.

the missile flight, so it is difficult to calibrate the scale through the advance calibration. When the scale coefficient between the detector, the frame angle sensor, and the angular rate gyro is equal, it will not lead to the isolation problem of the roll-pitch seeker. At this point, the scale coefficient K_g will only change the value of the proportional guidance coefficient N.

Due to the seeker scale deviation, the line-of-sight angle error caused by missile body disturbance will generate the wrong line-of-sight angular velocity and generate the wrong control instructions through the guidance law and pilot, thus generating additional missile body attitude movement, thus forming the isolation parasitic loop in the guidance loop. Figure 16 shows the guidance system model of the roll-forward seeker including the parasitic loop of isolation degree.

At the initial moment, when the missile is far away from the target, the influence of the external guidance loop on the stability of the guidance system is relatively small. The stability of the guidance system is mainly determined by the parasitic loop of DRR, and the parasitic loop can be selected separately for analysis. The block diagram of the parasitic loop of DRR of the inverted roll seeker is shown in Figure 17.

The seeker module in Figure 17 is replaced by the simplified model of the roll-pitch seeker, and the new module is shown in following formula:

$$\frac{x(s)}{y(s)} = \frac{k_1 k_2 s}{(T_1 s + 1)(T_2 s + 1)(T_3 s + 1)(s + k_2)}. \quad (22)$$

In this new equation, the seeker module adds some parameters. The values of these parameters have an impact

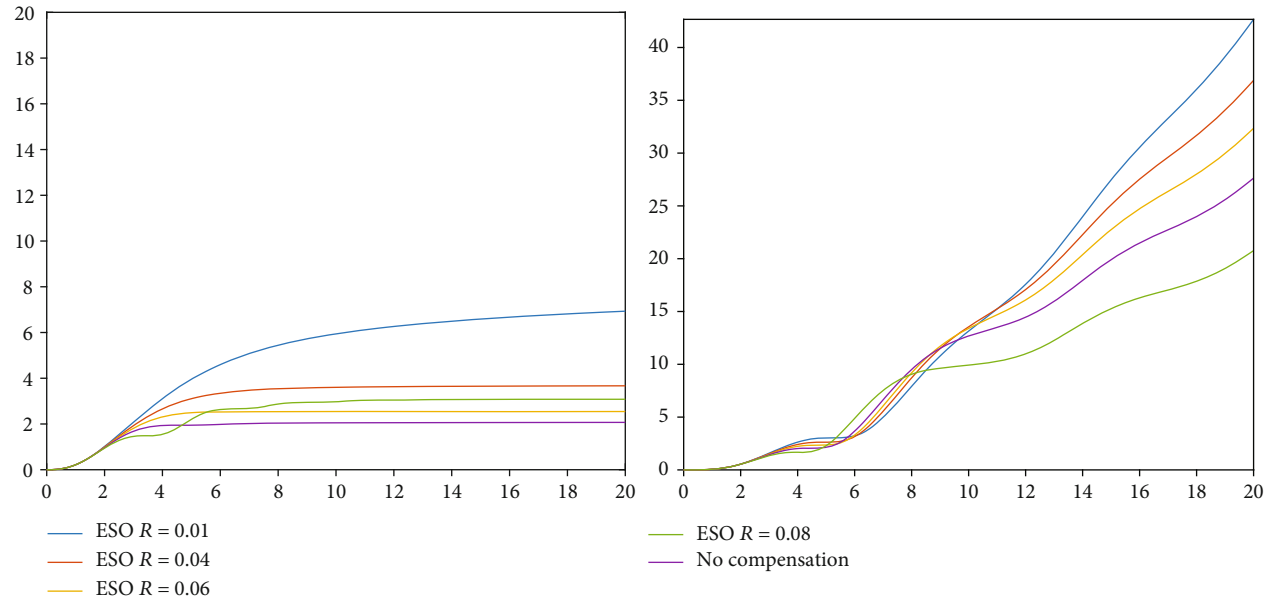

Figure 21: Effect of target random maneuver on dimensionless miss distance under step and wave disturbance.

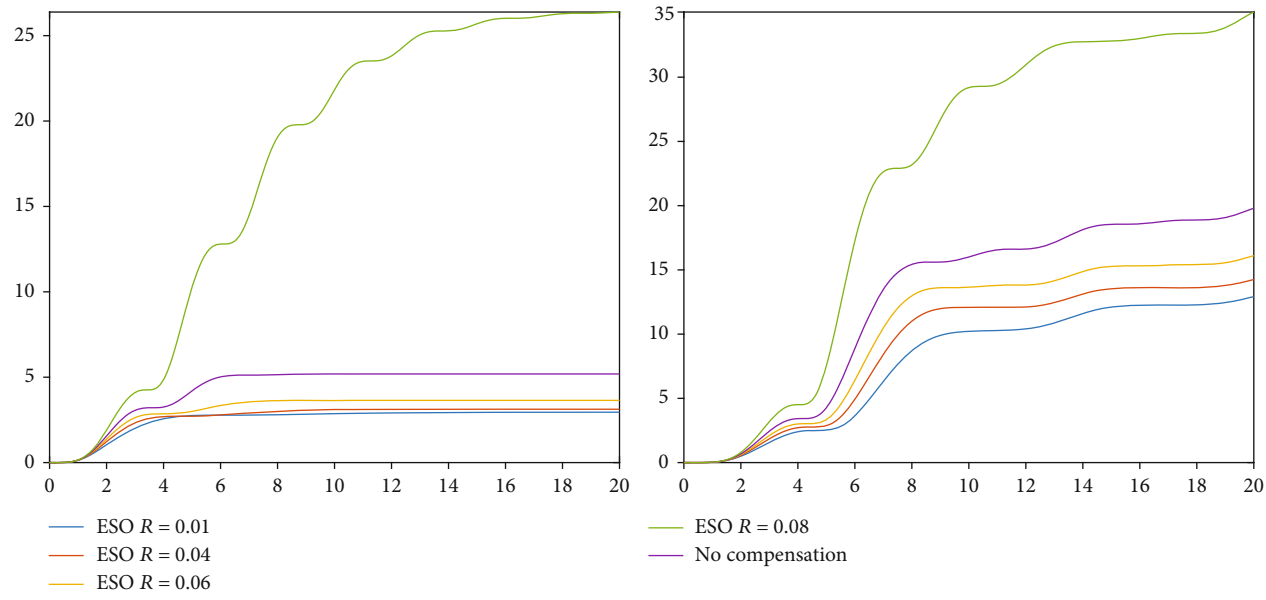

Figure 22: Effect of line-of-sight extraction on dimensionless miss distance under step and wave disturbance.

on the performance of the seeker. Referring to References [14, 15, 20, 22], we can set suitable values for these parameters. The specific meaning of parameters and the assignment of parameters in the simulation process are shown in Table 2.

For an air-to-air missile that uses a roll-pitch seeker for terminal guidance, its terminal guidance accuracy is affected by errors such as 5initial pointing error, target maneuver, and seeker measurement noise. According to the characteristics of the error source, the terminal guidance error source can be divided into two types: deterministic error and random error.

The deterministic error refers to the error whose size is known after the model is determined. The deterministic error that affects the final guidance precision mainly includes the initial pointing error and the target constant maneuver.

The initial pointing error is caused by the deviation angle of the missile's velocity vector, so that the missile has a velocity component in the direction of the vertical missile line, which will increase the deviation between the missile and the target in the direction of the vertical missile line. The ideal starting control condition of terminal guidance is that the initial pointing error is zero, at which point the missile can hit the nonmaneuvering target without control. However, it is

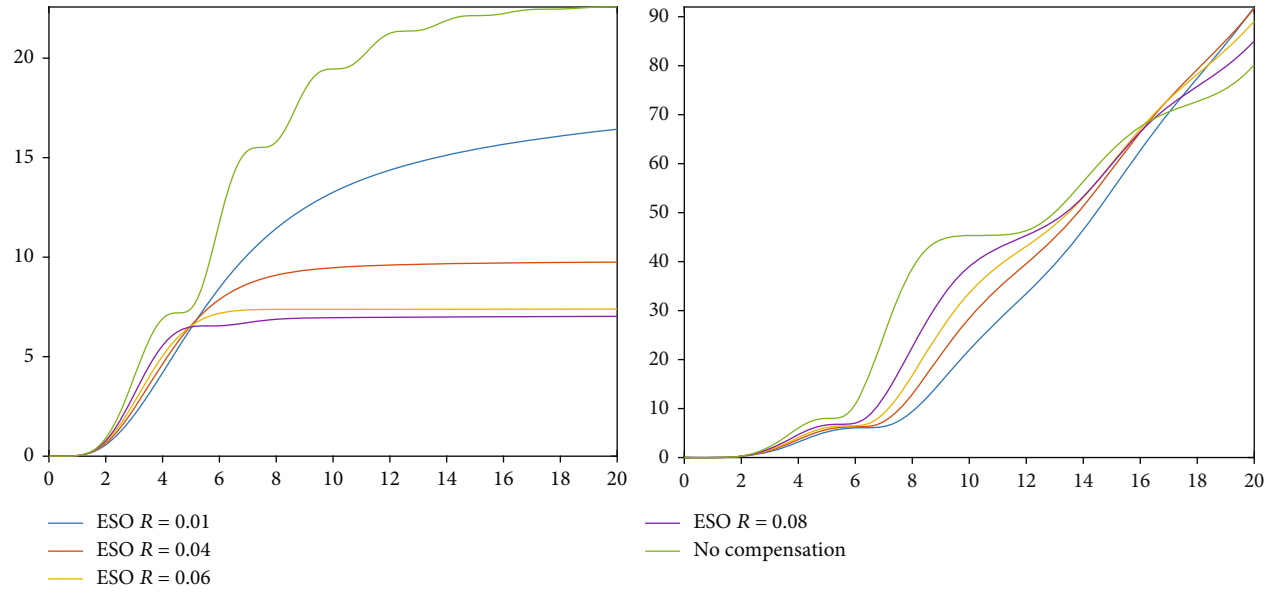

Figure 23: Effect of line-of-sight velocity extraction on dimensionless miss distance under step and wave disturbance.

difficult to do this in practical application, so the velocity deviation of the missile needs to be corrected by the guidance control system.

When intercepting an air target, the target usually maneuvers in the terminal guidance section. Target constant maneuver refers to the constant acceleration perpendicular to the line of sight of the missile. Random error is the uncertainty factor in terminal guidance. The random error which affects the precision of terminal guidance mainly includes target random maneuver and seeker measurement noise.

Considering the guidance control loop of the roll-pitch seeker with deterministic error and random error, the block diagram as shown in Figure 18 is established.

The relationship between dimensionless miss distance of the guidance control system with the ESO compensation method and dimensionless miss distance of the guidance control system without the ESO compensation method is obtained through simulation. The simulation results are shown in Figures 19–23.

Figures 19–23 show the relation between the dimensionless miss distance and ESO compensation method in the cases that the input disturbances are step disturbance and low frequency fluctuation. We can see from Figure 19 that, when the input disturbance is the initial point to the error, under the condition of step disturbance, dimensionless miss distance can converge to zero. In the nondimensional miss distance with the ESO compensation method, compared with that without the compensation method, convergence of nondimensional miss distance is smoother. The result is better when the DRR value is lower. In the case of wave disturbance, the situation is the same.

We can see from Figures 20–23 that, when the input errors are the constant target maneuver, the random maneuver, the line-of-sight angle error, and the line-of-sight angular velocity error, the step disturbance can make dimensionless miss distance converge to a fixed value. The

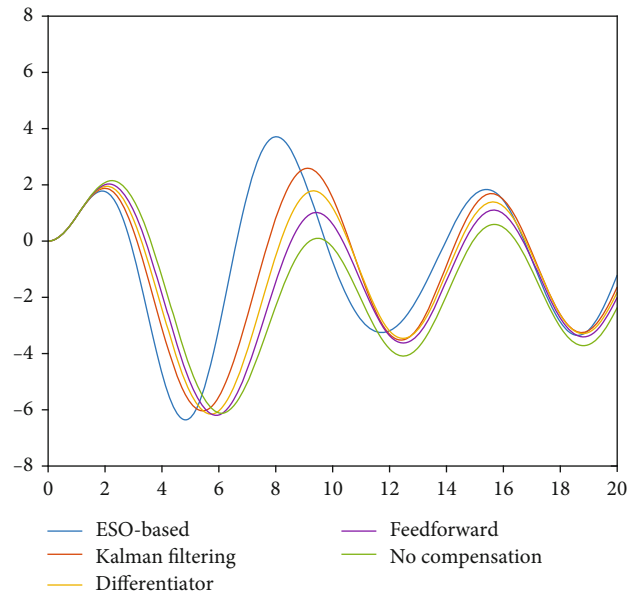

Figure 24: Effect of initial pointing error.

dimensionless miss distance using the ESO compensation method convergence process is more stable than that without using the compensation method. The dimensionless miss distance convergence rate is different if the effect of compensation methods is different. In the case of wave disturbance, the situation is the same.

For the simulation comparison of dimensionless miss distance under different compensation methods, random wave input is selected as the input of different error sources. The compensation results of different compensation methods are that the DRR values of the seeker system are different. Figures 24–28 show the simulation results of dimensionless miss distance under different compensation methods.

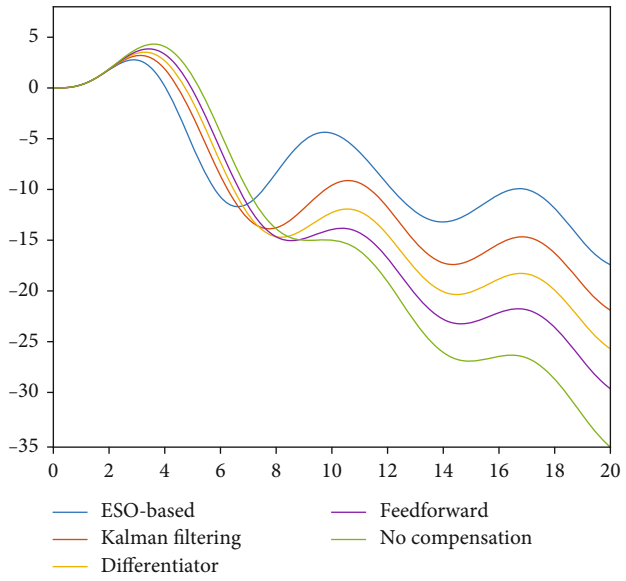

Figure 25: Effect of target constant maneuver.

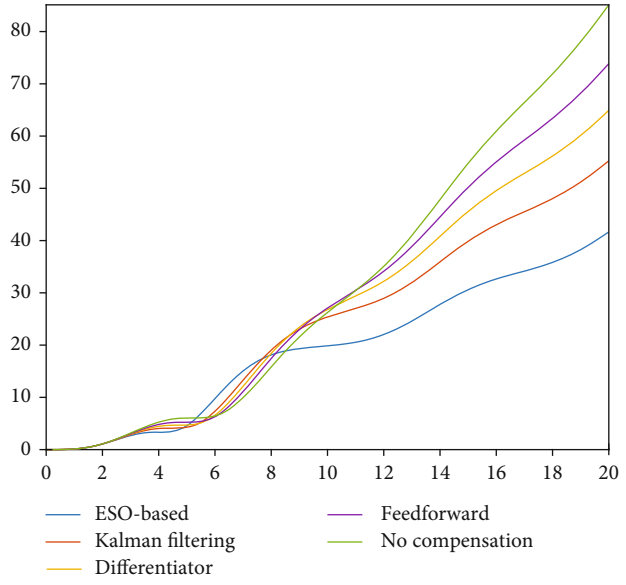

Figure 26: Effect of target random maneuver.

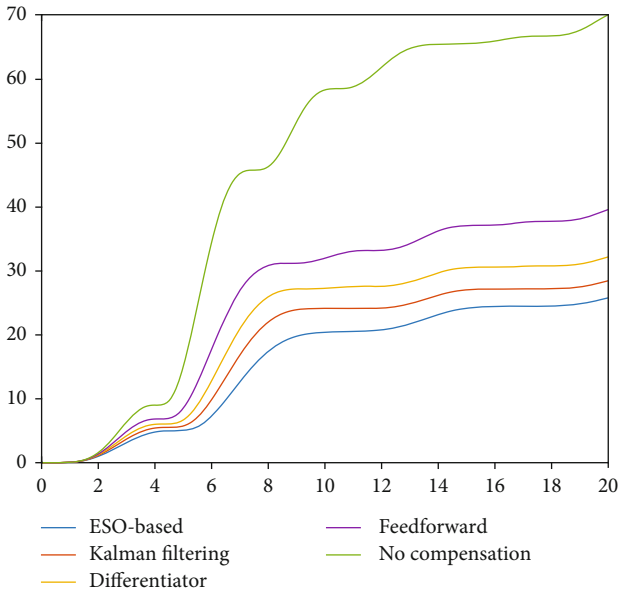

Figure 27: Effect of line-of-sight angle extraction.

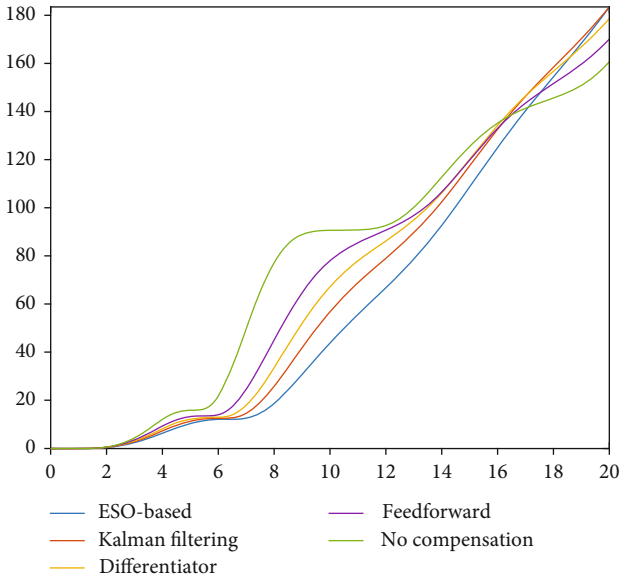

Figure 28: Effect of line-of-sight velocity extraction.

From Figures 24–28, we know that different DRR compensation methods have different effects on the dimensionless miss distance under various error input conditions. Different DRR compensation methods have different compensation effects for the air-to-air missile guidance system with the roll-pitch seeker, and the DRR values of the system after compensation are different. Through the analysis in Section 3, we know that under the same conditions, the DRR compensation effect of the ESO-based method is better than that of the Kalman filtering method, differentiator method, and feedforward method. The DRR compensated by different compensation methods can be obtained through simulation, which will be substituted into the guidance system, and the dimensionless miss distance is obtained through simulation. Simulation results show that the dimensionless miss distance of the ESO-based compensation method is smaller than that of other compensation methods.

5. Conclusion

By modeling the DRR compensation method of the two frames of the roll-pitch seeker based on ESO, we simulated and compared the compensation effect of the ESO compensation method on DRR under different interference torques and frequency bandwidths. The guidance loop system of the roll-pitch seeker containing the parasitic loop of DRR is established. Considering the influence of the ESO compensation method on dimensionless miss distance under different

error conditions, the following conclusions are obtained through experimental simulation:

(1) By studying the frame model of the roll-pitch seeker, it can be seen that the viscous damping moment, spring moment, counter potential moment, and other disturbing moments will all reduce the seeker's ability to isolate the disturbance of the warhead. For both of the roll frame and the pitch frame, the bigger the interference torque coefficient is, the weaker the seeker's ability to isolate the disturbance is. The isolation degree caused by viscous damping moment and spring moment can be compensated by the DRR compensation method based on ESO. Compared with the existing compensation method, the ESO-based method has a better compensation effect

(2) The frequency bandwidth of the seeker also affects the compensation effect of the ESO-based DRR compensation method. In the design range of the frequency bandwidth of the seeker, the larger the frequency bandwidth is, the better the compensation effect will be. In addition, the frame angular velocity after compensation is proportional to the interference torque. The larger the interference torque is, the larger the compensated frame angular velocity will be. The relationship between these two parameters is approximately linear

(3) For the guidance system with the DRR parasitic loop, when the input disturbance is the initial point error, under the condition of step disturbance, dimensionless miss distance can converge to zero. In the nondimensional miss distance with the ESO compensation method, compared with that without the compensation method, convergence of nondimensional miss distance is smoother. The result is better when the DRR value is lower. In the case of wave disturbance, the situation is the same. When the input errors are the constant target maneuver, the random maneuver, the line-of-sight angle error, and the line-of-sight angular velocity error, the step disturbance can make dimensionless miss distance converge to a fixed value. The convergence process of dimensionless miss distance using the ESO-based compensation method is more stable than that without using the ESO-based compensation method. The convergence rate of dimensionless miss distance is different if the effect of compensation methods is different. In the case of wave disturbance, the situation is the same

In addition, different DRR compensation methods have different effects on the dimensionless miss distance under various error input conditions. From the simulation, we know that the DRR compensation effect of the ESO-based method is better than that of the Kalman filtering method, differentiator method, and feedforward method. The dimensionless miss distance of the ESO-based compensation method is smaller than that of other compensation methods.

The research results can provide a reference for the performance research of the latest generation air-to-air missile based on the roll-pitch seeker. In addition, the research results can also provide help for the research of the roll-pitch seeker in different aspects, such as the parasitic loop, frame model, parameter design, guidance system design, error input model, and target maneuver model.

Data Availability

The data used to support the findings of this study are included within the article.

Conflicts of Interest

The authors declare that there is no conflict of interests regarding the publication of this paper.

Acknowledgments

This work is supported in part by research grants from the Key Laboratory Foundation, China (6142504200108).

References

[1] Y. Guo, J.-h. Guo, X. Liu, A.-j. Li, and C.-q. Wang, "Finite-time blended control for air-to-air missile with lateral thrusters and aerodynamic surfaces," *Aerospace Science and Technology*, vol. 97, p. 105638, 2020.

[2] G. Waldron, "Indian air-to-air missile pact puts MBDA on target," *Flight International*, vol. 196, no. 5705, 2019.

[3] M. R. Mortazavi and F. Almasganj, "Optimal midcourse guidance of an air-to-air missile via SVM and RVM," *Soft Computing*, vol. 23, no. 15, pp. 6603–6616, 2019.

[4] S. Lin, W. Wang, W. Lin, and C. Li, "The research of loop-shaping method to mitigate the total error effect in air- to-air missiles," *Optik*, vol. 181, pp. 923–932, 2019.

[5] H. Liu, M. C. Zhu, B. Liu, and H. G. Jia, "LOS stabilization and gyro configuration analysis for roll-pitch seeker," *Applied Mechanics and Materials*, vol. 2658, 2013.

[6] Z. Chen, K. Shi, N. Chen et al., "The experimental study about laser-induced dizziness effect of medium-wave infrared seeker which based on image processing," *Journal of Visual Communication and Image Representation*, vol. 59, pp. 401–406, 2019.

[7] Z. Ge, Y. Cheng, M. Xu, Y. Huang, S. Liu, and Y. Wang, "Study on distribution of magnetic field interference in infrared seekers and shielding plans," *Measurement*, vol. 132, pp. 336–343, 2019.

[8] S. Elbasuney, A. Elsaidy, M. Kassem, and H. Tantawy, "Infrared signature of novel super-thermite (Fe 2 O 3 /Mg) fluorocarbon nanocomposite for effective countermeasures of infrared seekers," *Journal of Inorganic and Organometallic Polymers and Materials*, vol. 28, no. 5, pp. 1718–1727, 2018.

[9] M. Zhang, H. Liu, H. Zhang, and X. Miao, "A hybrid control strategy for the optoelectronic stabilized platform of a seeker," *Optik*, vol. 181, pp. 1000–1012, 2019.

[10] X. Wang, B. Mo, X. Li, and S. Su, "Predictive functional control-based zenith pass controller design for roll-pitch seeker," *International Journal of Aerospace Engineering*, vol. 2020, Article ID 9709341, 12 pages, 2020.

[11] Z. Chen, N. Chen, K. Shi, G. Li, and X. Liu, "The research about high-dynamic and low-gray target image differential capture technology based on laser active detection," *EURASIP Journal on Image and Video Processing*, vol. 2018, no. 1, 2018.

[12] S. Liu, Z. Liu, S. Wang, and X. Qiu, "Research on influencing factors of detection accuracy based on laser seeker," *Journal of Physics: Conference Series*, vol. 1087, no. 5, 2018.

[13] Y. Zhang, "Strapdown optical seeker guidance instructions extraction and system stability," *Applied Mechanics and Materials*, vol. 2658, 2013.

[14] X. Du, R. Lv, H. Tu, and C. Jiang, "The research on infrared seeker with disturbance rejection effect parasitic," *Optik*, vol. 170, pp. 409–419, 2018.

[15] X. Wang, B. Mo, X. Li, and F. Liu, "A line-of-sight rate estimation method for roll-pitch gimballed infrared seeker," *Optik*, vol. 192, p. 162935, 2019.

[16] R. Bai, Q. Xia, and X. Du, "The study of guidance performance of a phased array seeker with platform," *Optik*, vol. 132, pp. 9–23, 2017.

[17] S. Liu, T. Lu, T. Shang, and Q. Xia, "Dynamic modeling and coupling characteristic analysis of two-axis rate gyro seeker," *International Journal of Aerospace Engineering*, vol. 2018, Article ID 8513684, 14 pages, 2018.

[18] K. Chen, Q. Xia, X. Du, Y. Yao, and C. Orlando, "Influence of seeker disturbance rejection and radome error on the Lyapunov stability of guidance systems," *Mathematical Problems in Engineering*, vol. 2018, Article ID 1890426, 9 pages, 2018.

[19] Y. F. Xu, Z. Y. Zhang, K. Li, and M. K. He, "Study of control algorithm for indirect stabilized optical seeker," *Applied Mechanics and Materials*, vol. 1082, 2011.

[20] L. Wei, L. Shixiang, Z. Wenjie, and X. Qunli, "On-line compensation for the disturbance rejection rate of a platform seeker based on a high-gain extended state observer," *International Journal of Aerospace Engineering*, vol. 2019, Article ID 3106732, 18 pages, 2019.

[21] W. Li, Q. Wen, and Y. Yang, "Stability analysis of spinning missiles induced by seeker disturbance rejection rate parasitical loop," *Aerospace Science and Technology*, vol. 90, pp. 194–208, 2019.

[22] X. Liu, B. Mo, and F. Liu, "Line-of-sight stabilization of roll-pitch seeker using differentiator-based disturbance compensation control," *Proceedings of the Institution of Mechanical Engineers, Part G: Journal of Aerospace Engineering*, vol. 234, no. 7, pp. 1326–1339, 2020.

[23] X. Du and Q. Xia, "The research of guidance performance of the phased array seeker with platform for air-to-air missile," *Optik*, vol. 127, no. 22, pp. 10322–10334, 2016.

[24] S. Liu, X. Du, and Q. Xia, "An on-line compensation method for the disturbance rejection rate of seekers," *Optik*, vol. 157, pp. 1306–1318, 2018.

[25] D. Gao, Q. Wang, Y. Lei, Z. Chen, and L. Shangguan, "Online real-time estimation of response time for periodic messages in controller area networks," *Mathematical Problems in Engineering*, vol. 2015, Article ID 659623, 13 pages, 2015.

[26] S.-Y. Lin, D. Lin, and W. Wang, "A novel online estimation and compensation method for strapdown phased array seeker disturbance rejection effect using extended state Kalman filter," *IEEE Access*, vol. 7, pp. 172330–172340, 2019.

[27] M. Bahreini and J. Zarei, "Robust finite-time fault-tolerant control for networked control systems with random delays: a Markovian jump system approach," *Nonlinear Analysis: Hybrid Systems*, vol. 36, 2020.

[28] C. Chongyang, Z. Song, W. Yongchang, and C. Chongyang, "Finite-time stability of delayed memristor-based fractional-order neural networks," *IEEE transactions on cybernetics*, vol. 50, no. 4, 2020.

[29] J. Zhang, Q.-G. Wang, and J. Sun, "On finite-time stability of nonautonomous nonlinear systems," *International Journal of Control*, vol. 93, no. 4, pp. 783–787, 2020.

[30] S. P. Bhat and D. S. Bernstein, "Geometric homogeneity with applications to finite-time stability," *Mathematics of Control, Signals, and Systems*, vol. 17, no. 2, pp. 101–127, 2005.

[31] Patents, "Signal processing device, touch panel unit, information processor, and signal processing method," in *Patent Application Approval Process*, Electronics Newsweekly, 2015.

[32] W. D. Xu, A. Wang, Z. J. Lv, H. Liu, and J. H. Wu, "Preliminary study of multiband smokescreen's interference with TV guidance," *Advanced Materials Research*, vol. 3530, 2014.

[33] D. E. Bellasi, L. Bettini, C. Benkeser, T. Burger, Q. Huang, and C. Studer, "VLSI design of a monolithic compressive-sensing wideband analog-to-information converter," *IEEE Journal on Emerging and Selected Topics in Circuits and Systems*, vol. 3, no. 4, pp. 552–565, 2013.

[34] D.-A. Nguyen, B. Cho, C. Seo, J. Park, and D.-H. Lee, "Analysis of the optimal frequency band for a ballistic missile defense radar system," *Journal of Electromagnetic Engineering And Science*, vol. 18, no. 4, pp. 231–241, 2018.